Mesoscopic modeling of the effect of branching on the viscoelasticity of entangled wormlike micellar solutions

Weizhong Zou,[1] Grace Tan,[1] Mike Weaver,[2] Peter Koenig,[2] and Ronald G. Larson[1,*]
[1]*Chemical Engineering, University of Michigan, Ann Arbor, Michigan 48109, USA*
[2]*The Procter & Gamble Company, Mason, Ohio 45040, USA*

(Received 8 August 2022; accepted 13 September 2023; published 9 October 2023)

The effect of branches on the linear rheology of entangled wormlike micelle solutions is modeled by tracking the diffusion of micellar material through branch points. The model is equivalent to a Kirchhoff circuit model with the sliding of an entangled branch along an entanglement tube due to the constrained diffusion of micellar material analogous to the flux of current in the Kirchhoff circuit model. When combined with our previous mesoscopic pointer algorithm for linear micelles that can both break and fuse, the model adds a branch sprouting process and therefore enables simulation of the dynamics of structural change and stress relaxation in ensembles of micelle clusters of different topologies. Applying this model to study the relationships between fluid rheology and microstructure of micelles, our results show that branches change the scaling law exponents for viscosity vs micelle strand length. This contrasts with the longstanding hypothesis that branches affect viscosity and relaxation in the same way that micelle ends do. The model also suggests a process for inferring branching density from salt-dependent linear rheology. This is exemplified by mixed surfactant solutions over a range of salt concentrations with flow properties measured using both mechanical rheometry and diffusing wave spectroscopy. By elucidating the connection between the branching characteristics, such as strand length and branching density, with the nonmonotonic variation of solution viscosity, the above model provides a powerful tool to help extract branching information from rheology.

DOI: 10.1103/PhysRevResearch.5.043024

I. INTRODUCTION

Surfactants, which are at the heart of many chemical and biological systems [1–6], spontaneously assemble into solution aggregates, including cylindrical micelles [7–9], driven by a delicate balance between the solvophilic and solvophobic parts of the molecule [10–14]. This balance also controls the densities of two types of thermodynamic defects in the cylindrical body of the micelle, namely, endcaps and branch junctions [15–17]. The resulting structure breaks, reforms, and exchanges surfactants at rates that determine the viscoelastic behavior of the surfactant fluid [18–22].

Over many decades, a rich variety of theories and models that allow micellar structure to be characterized from dynamic properties such as conductivity, light scattering, and viscoelasticity has been developed [16,23–30]. Among the available models, that of Cates *et al.* [1] for linear (unbranched) micelles has been particularly fruitful, for example, in providing a means of estimating from linear rheology the average micelle length $\langle L \rangle$, a property that is otherwise inaccessible when micelles are linear but entangled [5,7,29,31–33]. While the underlying Cates model appears to be sound, the earliest method of estimating micelle length was too simple to accurately account for the sensitivity of micellar structure, including its length and stiffness, on the presence of salts and additives [8,33–35]. Such deficiencies have been addressed by a mesoscopic simulation method, the pointer algorithm, applied to the Cates model by Zou and Larson [36] and Zou *et al.* [37]. The pointer algorithm provides a comprehensive description of disentanglement dynamics, micellar reactions controlling the average length of the micelle, as well as structural flexibility, in linear micelles [29,36–39].

For branched micelles, however, experimental detection of the presence and density of branch points is far more challenging. A variety of different methods, such as cryo-transmission electron microscopy (TEM), rheology (small amplitude oscillatory shear and extensional), neutron spin echo, and nonlinear flow measurements, have been used to detect micellar branches [40–46]. Although light and neutron scattering can provide evidence for topological branching when micellar solutions are dilute, their results, when extrapolated to the entangled regime, remain controversial due to the difficulty in distinguishing branched micelles from linear entangled networks [29,40,47,48]. On the other hand, cryo-TEM, which differentiates intersecting micelles from branches by their contrast in the transmitted electron beam, provides definitive evidence of branching [8,12,42,49]. Nevertheless, since micellar structures are labile to thermomechanical treatment [17,22,32,50], quantitative characterization of branch junctions by cryo-TEM (which mostly appear to be trifunctional

*rlarson@umich.edu

Y junctions) is sensitive to sample preparation [3,7,41,49,51]. In addition, unlike branched polymers, surfactants in a micelle can diffuse through their branch junctions, causing a change in the topological structure of both the entanglement network and the micelle itself, thus providing multiple routes for disentanglement and lowering the solution viscosity [31,52]. Since rheology is highly sensitive to branches, to quantify the effects of branching on the rheology of micellar solutions, the living architecture of a branched micelle needs to be modeled efficiently as an evolving set of linear strands that are connected by multiple junctions and terminated by multiple ends.

In this paper, we extend our previous mesoscopic pointer algorithm for entangled linear micelles that can both break and fuse, to include branching into treelike clusters of arbitrary complexity. This is achieved through a constrained diffusion model, such as that of Lequeux [53], which draws on the idea that reptationlike intramicellar diffusion produces a flux of micellar material through each strand, even as it remains confined within its entanglement tube. The accommodation of the pointer algorithm to a branch sprouting process is also explained thoroughly, where the method for moving pointers is guided by advanced tube theories. A factorial design of computations by varying micellar parameters demonstrates a change of scaling law exponents for viscosity as a function of branching level, in contrast with a longstanding hypothesis that branch points affect viscosity the same way micelle ends do. The effect of branching was also studied experimentally through a serial of mixed surfactant solutions containing both sodium lauryl one ether sulfate (SLE1S) and cocamidopropyl betaine (CAPB) over a range of salt ion concentration. By combining mechanical rheometry and diffusing wave spectroscopy (DWS) for viscoelastic characterization, the above model enables a quantitative evaluation of relationships between fluid rheology and microstructure of micelles.

II. MODELING AND SIMULATION

A. Constrained diffusion and branched micelle architecture

While the model of Lequeux [53] produced a simple equivalence between the effect of branch points and chain ends on the overall rheological response, we develop here a quantitative model by extending the pointer algorithm to branched micelles. We do so by defining a micellar *strand* as the linear portion of a micelle terminated by either a free end or a branch point at each end of the strand. We satisfy overall mass conservation by imposing a constraint force at each strand terminus so that the resulting linear displacement Δx_{ij} (from i to j) of the micellar strand bounded by termini i and j is given by a Langevin equation:

$$\Delta x_{ij} = \sqrt{\frac{6k_BT\,\Delta t}{\zeta_{ij}}}\,n_{ij} + \frac{F_i - F_j}{\zeta_{ij}}\Delta t, \tag{1}$$

where Δt is the time step, ζ_{ij} is the drag coefficient for strand (i, j), and n_{ij} is a uniformly distributed random number between -1 and 1. Note that the first and second terms on the right side of Eq. (1) represent the intramicellar diffusion and the effective constraint at terminus i and j, respectively. The nonzero constrained force F_i at the junction can be understood as the fluctuating potential that arises from imbalances of material flux in each strand that would occur in the absence of this potential. Thus, the contribution from this intramicellar diffusion to the structural lability of branched micelles (the length and the number of the strands in a branched micelle change with time) can be captured by a model of constrained reptation: The overall diffusion of surfactant molecules in each strand creates a random flux of micellar material along entanglement tubes or an analogous current in the Kirchhoff circuit model of Fig. 1.

Assuming that the effect of the terminus geometry on the rate of constrained diffusion is small, ζ_{ij} will be proportional to the strand length ($= \zeta_0 L_{ij}$, ζ_0 is drag coefficient per unit length of micelle), and branch points then act as pointlike objects. Since no mass can accumulate at a junction, if a net inward current were to occur there, a high potential just large enough to suppress this current would be produced. After numerically labeling the junctions and taking free ends as junctions with zero potential, the material flux of Eq. (1) in each arm is rewritten below in a connectivity matrix for the branched micelle with the architecture of a 3-arm in Fig. 1:

$$\begin{bmatrix} 1 & 0 & 0 & a_{41} & 0 & 0 & -a_{41} \\ 0 & 1 & 0 & 0 & a_{42} & 0 & -a_{42} \\ 0 & 0 & 1 & 0 & 0 & a_{43} & -a_{43} \\ 0 & 0 & 0 & 1 & 0 & 0 & 0 \\ 0 & 0 & 0 & 0 & 1 & 0 & 0 \\ 0 & 0 & 0 & 0 & 0 & 1 & 0 \\ -1 & -1 & -1 & 0 & 0 & 0 & 0 \end{bmatrix} \begin{bmatrix} \Delta x_{41} \\ \Delta x_{42} \\ \Delta x_{43} \\ F_1 \\ F_2 \\ F_3 \\ F_4 \end{bmatrix} = \begin{bmatrix} b_{41} \\ b_{42} \\ b_{43} \\ 0 \\ 0 \\ 0 \\ 0 \end{bmatrix}, \tag{2}$$

where $a_{ij} = \frac{\Delta t}{\zeta_{ij}}$, $b_{ij} = \sqrt{\frac{6k_BT\,\Delta t}{\zeta_{ij}}}\,n_{ij}$.

In the above, a two-dimensional matrix represents the connectivity among all the strands in a micelle cluster regardless of the overall complexity of the micelle. The fourth to sixth rows in the connectivity matrix correspond to the three dangling ends with zero constrained forces (i.e., $F_1 = F_2 = F_3 = 0$), while the seventh row imposes the constraint of no mass loss or accumulation at the branch point.

The transport described by Eq. (2) for a multibranched micelle is thus equivalent to that of a Kirchhoff circuit in Fig. 1(b), with the micelle topology mapped onto a bidirectional connectivity matrix with randomly fluctuating voltages. Such a mapping permits micelles of arbitrary branch structure to be modeled, including multiple levels of treelike branching, as well as internal reconnections or loops. Equation (2) or its generalization to a micelle with many branch points can then be solved by the conventional numerical tools, such as LU decomposition. An analogous matrix is constructed for each branched or linear micelle in the ensemble, where a linear micelle has only one strand and two free ends and so is described by a 3×3 matrix. A complex treelike micelle is described by a large $(2n + 1) \times (2n + 1)$ matrix, where n is the number of strands. For a typical simulation of on average 5 branch junctions per micelle, the associated matrices of the largest micelle can easily become 50×50.

B. Micellar breakage and fusion

Micelles change their conformations or relax by both constrained diffusion and changes in the topology, without latter the strands deep inside a treelike cluster would relax only after

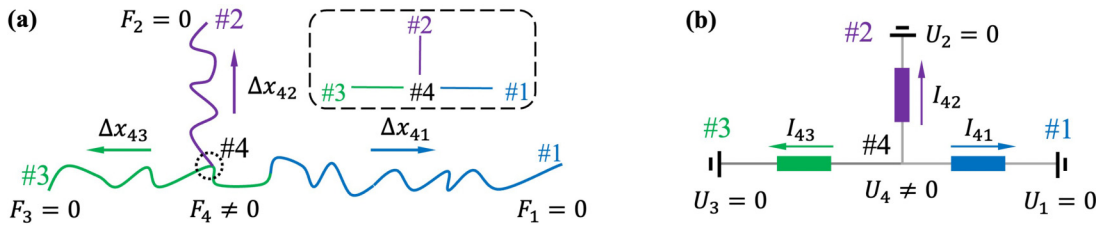

FIG. 1. (a) A 3-arm branched micelle architecture with symbols described by the text and Eq. (1) as well as (b) the corresponding Kirchhoff circuit with rectangular resistors representing strands and electrical grounds representing ends.

relaxation of peripheral branches. However, this relaxation in a hierarchical manner is greatly accelerated by breakage and fusion of micelles, which occur at a rate $k_{\rm br}$ (i.e., the breakage rate per unit micelle length) with equal probability at any point along the micelle. The simulations preserve the initial average mass or total length $\langle M \rangle$ of all strands of a micelle by stochastically introducing a fusion of two randomly chosen micelles each time a breakage occurs in any micelle, so that $\langle M \rangle$ is by definition the equilibrium micelle size. Thus, $k_{\rm br}$ and $\langle M \rangle$ together set the fusion rate per micelle. These breakage and fusion reactions are illustrated in Fig. 2, which defines the notation system that allows the micellar connectivity of arbitrary complexity to be specified. Breakage of a strand requires introduction of two new ends, which are assigned unused numbers [#15 and #16 in Fig. 2(a)], while fusion eliminates two ends [#4 and #17 in Fig. 2(b)], and these numbers are then available for reuse.

C. Micellar bud sprouting

To compensate the gradual loss of branches due to the constrained diffusion, new branches are randomly added as infinitesimal buds (with the size of micelle diameter ∼4 nm), as shown in Fig. 3(a), with equal probability per unit strand length, at a rate given by the inverse of a newly introduced time scale $\bar{\tau}_{\rm bud}$. That is, over time, every segment in a strand is given an equal probability to form a bud. Micelle branches form as a result thermal fluctuations of local curvature, which we model by sprouting or growing of those buds [50,54]. As illustrated in Fig. 3(b), any unsprouted bud, i.e., a bud that shrinks rather than grows on the subsequent time step (∼1 μs) by constrained diffusion, is annihilated, while a sprouting bud that grows on the next time step either becomes a short branch, as shown in Figs. 3(c) and 3(d), or fuses with another micelle, as shown in Fig. 2. Any time a branch arm shrinks by constrained diffusion to a negative length, it is removed. The continual addition of buds or potential branch junctions balances their destruction by constrained diffusion, leading in time to an equilibration of the branching density.

Closed intramicellar loops, which can occur occasionally via random end-to-end fusion of highly branched strands, should have relatively small effects on the properties of branched micellar systems except near a phase transition to a dense gel state (i.e., an interconnected network), where the mean-field description of our model fails. Although other

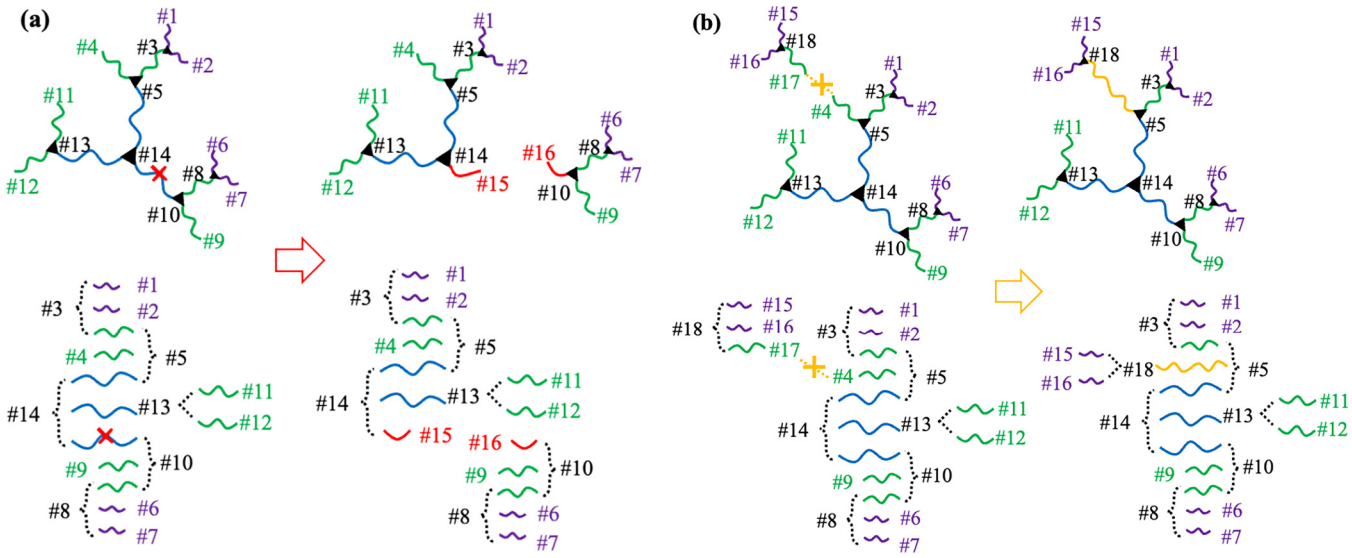

FIG. 2. The micellar breakage and fusion represented by the manipulation of the strand lists between branched clusters: (a) breakage and (b) recombination. The numbers identify chain ends and branch points. Each strand is thus defined by two numbers, one for each end or branch point. In the lower panel in (a) and (b), each bracket pairs a single number on the outside of the bracket identifying the branch point, with the three numbers on the inside of the bracket identifying the other ends of each of the three strands linked to that branch point. Each of these strands can itself be a branch point, as in the case of strand (13,14), which is bounded at both ends by branch points.

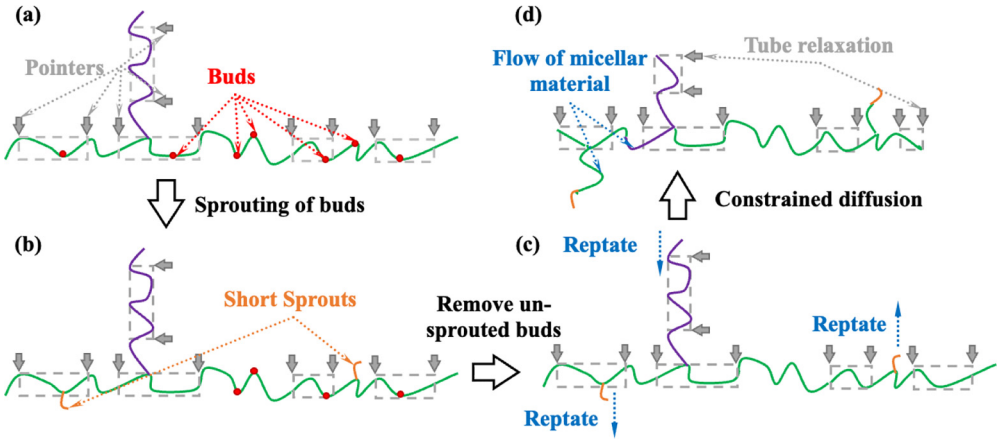

FIG. 3. The relaxation of branched micelles represented by the movement of pointers in the presence of (a) budding and (b) sprouting (growing) of new branches with constrained diffusion, as described in the text. Pointers are described by gray solid arrows along a micellar strand with each dashed rectangular region between two pointers representing an unrelaxed tube. Tube elements shrink between (c) and (d) due to diffusion of a green and purple branch endpoint into their respective tube segments, feeding micellar material into the growth of orange sprouts that first appeared in (b).

mechanisms of branch formation and change of micelle length, such as end splitting and interchange, strand-strand cross-linking, etc. [1,50,54], could be included in our model, we neglect them here, as their effects can likely be captured through modification of the effective rates of strand fusion/breakage and of budding/unbudding.

D. Evolution of pointers and relaxation mechanisms

Pointers are used to mark the boundaries between unrelaxed and relaxed point of micellar materials. Over time, the unrelaxed portions between pointer pairs shrink, and eventually, the two pointers meet each other and are removed from the strand, marking completion of the relaxation of that portion. Updating the number and positions of the pointers for each strand, the time-dependent normalized stress relaxation $\mu(t)$ can then be calculated as the fraction of micellar tube segments l_e that are unrelaxed at a given time t. Fast dynamics at time and length scales smaller than l_e, such as local Rouse and bending motions, are not captured by movement of the pointers but are added later using analytical formulas, as described in earlier publications [36–38,48], thus avoiding the unnecessary computational cost of tracking them explicitly. A detailed description of the above pointer algorithm can be found in our previous publications [36–38,48].

Unlike linear micelles, relaxation of branched micelles, as illustrated in Figs. 3(c) and 3(d), includes constrained diffusion under which the movement of the micelle allows pairs of pointers to gradually move toward each other, representing stress relaxation. This continues along dangling ends, which can be created by either micellar breakage or sprouting of a bud. However, pointer movement is not permitted along inner backbones that are terminated with branch junctions at both ends. Therefore, movement of a pointer along a dangling end must halt when the free end fuses with another free end to create a new backbone strand. This halting of pointers on a strand occurs even as the micellar material along that strand continues to flow into other strands by constrained diffusion since the stress is stored in the tube segments, not the micellar material. Strand breakage creates new dangling ends and releases pointers on that strand to move again. Thus, by tracking the unrelaxed portions of micelles (marked by pointers), the above pointer algorithm provides the only opportunity at present to simulate the linear viscoelastic properties of well-entangled branched micellar solutions with a hierarchy of length and time scales.

E. Simulation setup and equilibration

A typical simulation starts by equilibrating an exponential distribution of linear micelles [55–57] of average length $\langle L\rangle_{\text{in}}$ via micellar reactions, constrained diffusion, and bud-sprouting processes. To obtain robust statistics, $N = 2000$ micelles, initially all linear, are used, each of which may grow into branched micelles that can consist of multiple strands. Like our previous work on linear micelles [36–38,48], a unit length l_s, comparable with the persistence length l_p, is used to discretize the locations of breakage and budding points along the micelle. A cutoff length $L^c = 5\langle L\rangle_{\text{in}}$ is also chosen as the maximum initial micelle length allowed in the ensemble to prevent the appearance of giant micelles with probability $< 0.5\%$ in the ensemble. Given the total number N of micelles and maximum allowable length L^c in the initial linear ensemble, l_s can be chosen such that its value (see Eq. (S6) in the Supplemental Material [58]) has minimal effect on the macroscopic relaxation, as confirmed by our simulations. Details regarding simulation setup and data processing can also be found in the Supplemental Material [58].

As illustrated in Fig. 4(a), branched micelles are formed from initially linear micelles during the equilibration. To increase the efficiency in approaching equilibrium while avoiding the artificial effects of imposing rigid cutoffs, two dynamically varying cutoffs are set, i.e., the maximum allowed number of branched junctions per micelle J^c and the maximum length of a strand contained in a micelle S^c. Here, J^c $(= 5\langle J\rangle = 5\beta\langle M\rangle)$ and S^c $(= 5\langle S\rangle)$ vary

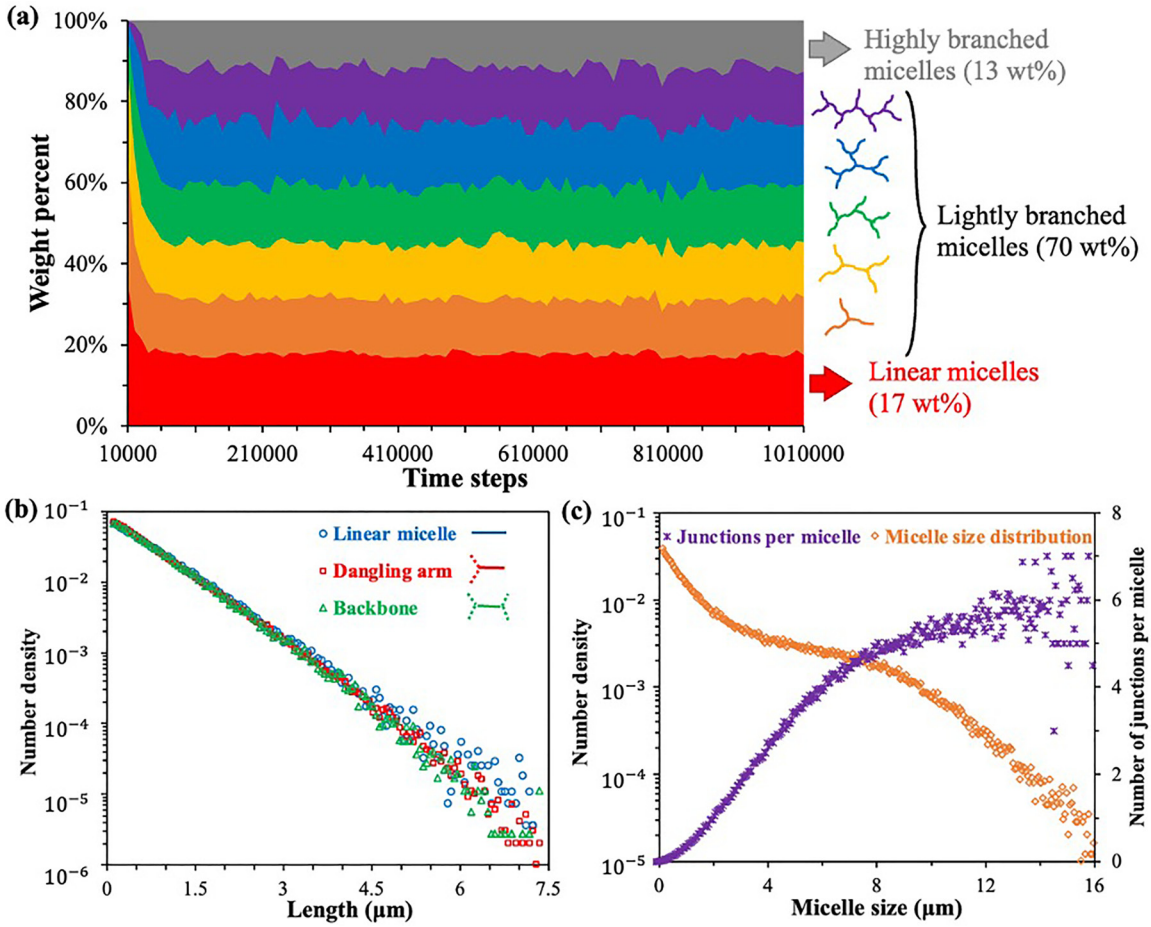

FIG. 4. (a) Evolution of micelle ensemble showing attainment of the well-equilibrated composition with final average strand length $\langle S\rangle = 0.645$ μm and branching level $\beta = 0.595$ per μm. Note that the equilibration starts from an ensemble of linear micelles of average size $\langle L\rangle_{\rm in} = 2.50$ μm with breakage/fusion time $k_{\rm br} = 4.0$ per μm of micelle, semiflexibility $\alpha_e = 2$ (the ratio of the entanglement length l_e to the persistence length l_p), and $l_p = 50$ nm. After equilibration, this yields (b) the strand length distribution and (c) the micelle number density and number of branched junctions per micelle as functions of micelle size. Note that, in (b), the overlap of three different types of strand length distribution plus their linearity on a semilog plot are the result of their creation by a Poisson random process, while (c) shows that the distributions of micelle size become noisy for giant micelles ($M > 10$ μm) due to the small number of them in the ensemble.

dynamically during the simulation in response to changes in their corresponding ensemble-averaged values. With equal rates of stochastic breakage and fusion events, the equilibration process holds the average micelle size $\langle M\rangle$ or length of all strands of a micelle fixed, and $\langle M\rangle = \langle L\rangle_{\rm in}$ (the averaged length in the initial linear ensemble before equilibration) which remains fixed because of the equal rates of micelle breakage and micelle fusion imposed by the algorithm. Due to the stochastic nature of creation and destruction of branch junctions and ends, at equilibrium, the length of a micelle strand must obey a Poisson (i.e., exponential) distribution with identical average length $\langle S\rangle$ regardless of its type, i.e., whether it is a linear micelle, a dangling arm, or an inner backbone, as shown by Fig. 4(b). The overall micelle size distribution, in Fig. 4(c), contains both many micelles that are too short to have many branches as well as a few, but very large, micelles with multiple branches due to fusion at a rate proportional to the number of branch ends. Since $\langle S\rangle$ and the branching density β are independent equilibrium parameters, empirical correlations to better guess their values from $\langle M\rangle$ and the budding time $\bar{\tau}_{\rm bud}$ (a kinetic parameter), which must be set before equilibration, are established as elaborated in the Supplemental Material [58].

III. MATERIALS AND EXPERIMENT

A. Materials

To infer the presence of branches by examining the changes in linear rheology with added salt, a series of micelle solutions was made with the same volume fraction ($\phi = 4.02\%$) but various concentrations of NaCl (with the total counterion concentration $[Na^+]$ from both salt and surfactant ranging from 0.801 to 1.101 M). The surfactant solutions contain two types of surfactants, SLE1S and CAPB, along with a simple salt (sodium chloride, NaCl). SLE1S [see Fig. 5(a)] is an abbreviation for commercial sodium lauryl ethylene glycol sulfate (SLES, industrial grade) with one ethoxyl group (EO) on average (but with a distribution of the number of EOs ranging from 0 to 10). CAPB [see Fig. 6(b), industrial grade] is a zwitterionic cosurfactant. The weight ratio of SLE1S/CAPB

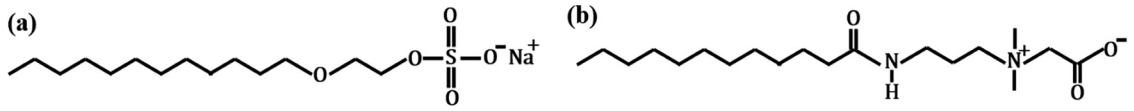

FIG. 5. The chemical structure for (a) sodium lauryl one ether sulfate (SLE1S) and (b) cocamidopropyl betaine (CAPB).

in the solution is fixed at 8.57. The activity of the SLE1S paste was verified using potentiometric anionic surfactant titration, ASTM D4251. All the samples were then well mixed at ratios designed to produce the desired surfactant and salt concentrations in the Supplemental Material [58] and allowed to rest overnight for degassing prior to measurements.

B. Macrorheology

An MCR-702 TwinDrive rheometer (Anton Paar) equipped with a 50-mm-steel 0.5° cone and plate was used for measurements. The zero-shear viscosity was measured in a flow experiment at low frequency, where a low-shear viscosity plateau was observed. The frequency sweep measurements were conducted with logarithmic variation in the applied strain amplitude through a built-in RheoCompass software. Such a variation in the strain amplitude maximizes the torque signal at lower frequencies while minimizing the effects of inertia at high frequencies within the linear viscoelastic range of the samples. The counterrotation mode was also used to divide the total strain amplitude between the upper and lower drive which helps limit inertial effects at high frequencies. The drive, system geometry, and motor were all calibrated or corrected prior to measurement. Only data where the measured torque deviates from the lower-drive-electric torque by $<2\%$ were included (which is the recommended criterion by Anton Paar). We sampled 10 data points per decade of frequency to obtain enough information in a reasonable time. Samples were freshly loaded each time, and a solvent trap was used to prevent solvent evaporation near the edge. All rheological measurements were performed within the linear viscoelastic regime at 25 °C. Each sample was remeasured, and the standard deviation of each rheological measurement was found to be $<5\%$.

C. DWS

As an optical microrheology approach, DWS was also applied to observe the high-frequency behavior ($10-10^5$ rad/s) of micelle solutions. Details about DWS can be found in Refs. [30,37,48,59]. The wavelength of light used in the DWS was 532 nm. Solutions of sulfate latex particles (8.2 wt.%, analytical grade, from Life Technology) with a bead size of 600 nm were used as molecular probes with final bead concentration at 0.5 wt.%. These beads, made of IDC polystyrene latex with a hydrophobic surface, were stabilized with a low level of sulfate charges (thus rendering the beads negatively charged) and were surfactant free. The samples for DWS measurement were well mixed with 0.5 wt. % beads before adding 10 wt. % NaCl solutions to avoid shocking of the samples. A high-speed vortex mixer was also used to ensure the homogeneity of the samples. After 12 h of equilibration, scattering from the sample was measured in a 5 mm glass cell on an LS Instruments RheoLab 7.1.0 system. The transport mean free path l^* (=552 μm) was determined from the control sample with the same size beads in water.

D. Combining mechanical rheology with DWS

When combining the high-frequency rheological data from DWS with the lower-frequency data from mechanical rheometry, ideally, the two sets of data should overlap at intermediate frequencies (10–100 rad/s). However, it is now well accepted

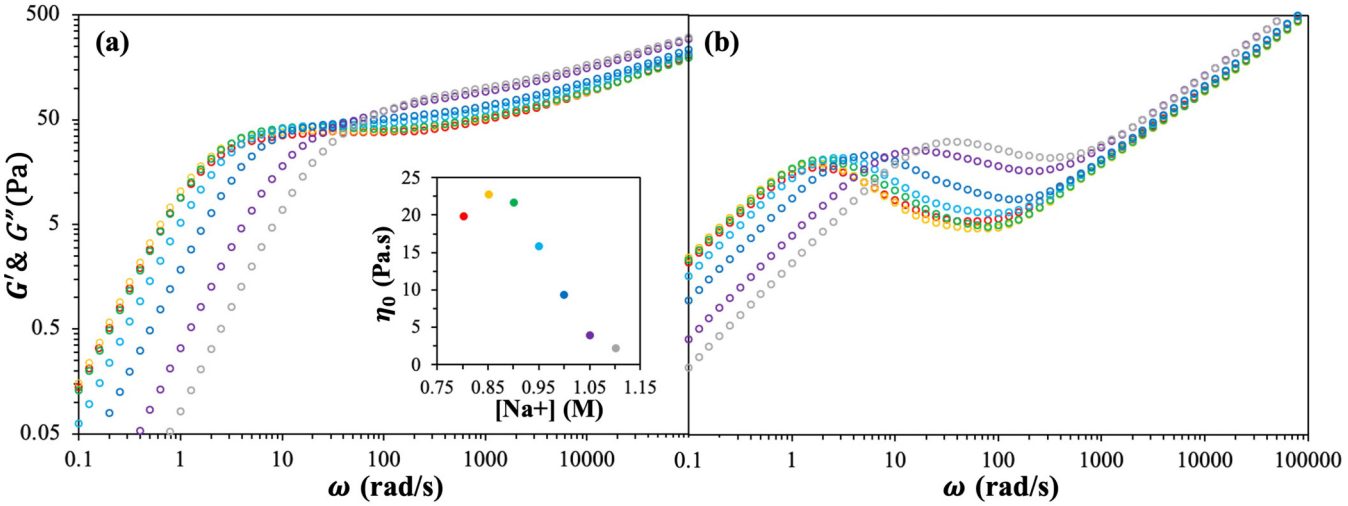

FIG. 6. The experimental measurements for (a) G' and (b) G'' of micelle solutions with the same surfactant volume fraction [4.04% sodium lauryl one ether sulfate (SLE1S) + cocamidopropyl betaine (CAPB)] but different concentrations of [Na^+]. The corresponding values of η_0 is plotted in the inserted plot, each coded with the same color as the corresponding rheological curves.

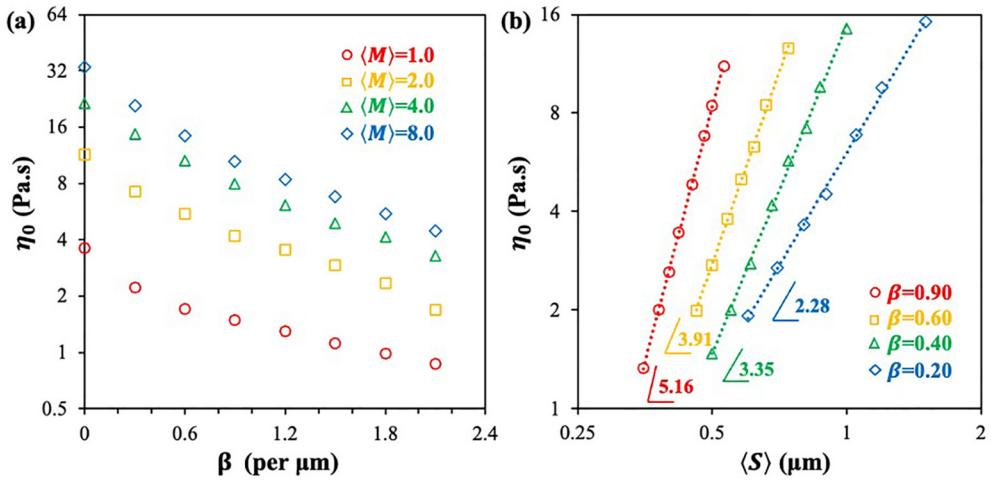

FIG. 7. Dependence of zero-shear viscosity η_0 as a function of (a) branching density β at a series of fixed micelle sizes $\langle M\rangle$ (in μm) and (b) average strand length $\langle S\rangle$ at fixed β. The dotted lines in the log-log plot of (b) are power law fits with the exponent indicated. Note that η_0 values are extracted from the terminal regions of G' and G'' curves given by Fig. S5 in the Supplemental Material [58] with breakage rate $k_{\rm br} = 4.0$ per μm of micelle, semiflexibility $\alpha_e = 2$, and persistence length $l_p = 50$ nm. $\langle M\rangle$ can be calculated from the values of $\langle S\rangle$ and β since only two of these parameters are independent. Small statistical errors (1–2%, shown in Fig. S6 in the Supplemental Material [58]) and obtained by repeating simulations (see Supplemental Material [58] for details) are within the size of the symbols.

that the microrheology overestimates or underestimates the elastic modulus due to slip and the compression of fluid at the interface between particle probe and viscoelastic medium as well as the formation of particle-micelle aggregates [2,59]. Consequently, to merge DWS data with the mechanical data requires that the magnitudes of G' and G'' from DWS be shifted by a factor that depends on the specific frequency range over which the two datasets overlap. The following procedure is therefore used to obtain the combined G' and G'' curves: (a) Mechanical rheometric data outside of a frequency window of 0.5–100 rad/s was removed, beyond which the data are subject either to the effect of inertia (at high frequency) or to low signal-to-noise ratio (at low frequency). (b) Truncation of DWS data is carried out at low (<10 rad/s due to poorly resolved terminal behavior) and high frequency ($>20\,000$ rad/s due to the limitation of Brownian motions of probe particles). (c) The remaining DWS data are eventually shifted vertically to allow for the best overlap with those from mechanical rheometry at frequencies between 50 and 150 rad/s. The resulting 6-decade frequency spectrum of rheological moduli G' and G'' for a 4.04% SLE1S + CAPB solution is obtained with the corresponding η_0 shown in Fig. 6.

IV. RESULTS AND DISCUSSION

A. Scaling behaviors for micellar viscosity

Given the details on data acquisition and the associated time-to-frequency transformation in the Supplemental Material [58], the flow properties of a micelle solution can be simulated for a well-equilibrated ensemble containing 2000 micelles, each of which may contain multiple and hierarchical branches. In Fig. 7, we present scaling laws of the zero-shear viscosity η_0 (extracted from the terminal region of G' and G'' curves, see Supplemental Material [58] for details) as functions of a set of micellar parameters including strand length $\langle S\rangle$, branching density β, and the average size of micelle $\langle M\rangle$. In Fig. 7(a), we find that viscosity decreases with increasing β for fixed micelle size $\langle M\rangle$. Thus, as the span of the micelle from one end to the other is decreased, a micellar segment has a shorter distance to slide by reptation to get from the interior of the micelle to its exterior, where it can relax. Thus, our results confirm the prevalent idea that relaxation is accelerated and viscosity is decreased in branched micelles relative to linear micelles of the same overall size $\langle M\rangle$ by the sliding of material through junctions [27,53,60]. However, Fig. 7(b) shows the increase in zero-shear viscosity η_0 with increasing average strand length $\langle S\rangle$ is much steeper at larger branch density β. This contradicts the conclusion of Khatory *et al.* [52] Lequeux [53], and Lequeux and Candau [60] that this dependence should be independent of β, i.e., the viscosity of a solution of branched micelles with average strand length $\langle S\rangle$ should be the same as that of a solution of linear micelles with average length $\langle S\rangle$. An intuitive explanation for the above steepening of the power law with increasing β is that an increase in $\langle S\rangle$ for a highly branched system adds exponentially to the micellar material located far from the high-mobility micelle ends and thus is slower to relax.

B. Effect of micellar breakage/fusion on solution viscosity

The effects of micelle breakage/fusion time $\bar{\tau}_{\rm br}$ (equivalent to $1/k_{\rm br}\langle M\rangle$) on η_0 and the corresponding rheological moduli G' and G'' of branched micelles are illustrated in Fig. 8. The increase of viscosity with increasing $\bar{\tau}_{\rm br}$ shows a power-law exponent of 0.48, which is consistent with that of the Cates theory (0.5) for linear micelles [55,56]. We find that the average strand length $\langle S\rangle$ and branching density β are nearly unaffected by a change in the breakage/fusion rate in Fig. 8, which is anticipated given that $\bar{\tau}_{\rm br}$ is a kinetic rather than a thermodynamic parameter. Here, G' and G'' shift horizontally with increased $\bar{\tau}_{\rm br}$ except at very high frequencies, where an overlap is observed. This indicates that the relaxation can be

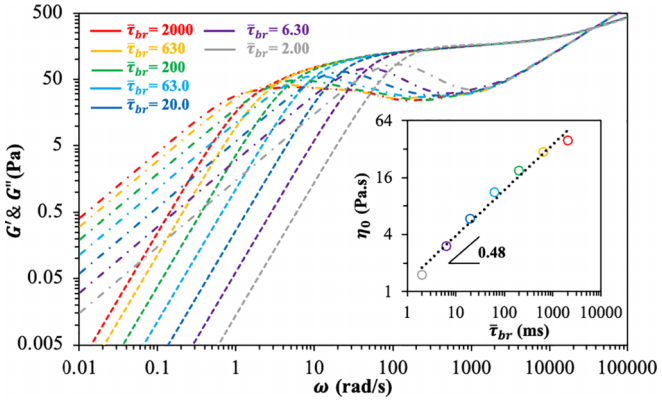

FIG. 8. The effects of micellar reaction time $\bar{\tau}_{\rm br}$ (s) on zero-shear viscosity η_0 (inserted plot), with each point given the color also used to plot G' (dashed lines) and G'' (dot-dashed lines) vs frequency ω for branched micelles with identical average strand length $\langle S\rangle = 0.96$ μm and branching level $\beta = 0.38$ per μm. The ensemble for these simulations was obtained by equilibrating a linear micelle ensemble of average size $\langle M\rangle = 3.50$ μm with $\tau_{\rm bud} = 0.2$ ms, semiflexibility $\alpha_e = 2$, and persistence length $l_p = 50$ nm. The upward shift of G'' with increasing $\bar{\tau}_{\rm br}$ at low frequencies yields the increase of η_0 with a power-law exponent of 0.48 ($R^2 = 0.963$) in inserted panel.

effectively accelerated by increasing $k_{\rm br}$ (i.e., by decreasing $\bar{\tau}_{\rm br}$), but the microstructure of the micelles remains unaffected when the semiflexibility ratio α_e (the ratio of entanglement to persistence length l_e/l_p) and the persistence length l_p are held constant. In other words, the breakage/fusion time $\bar{\tau}_{\rm br}$ reflects the living character of the micellar solution, whose magnitude can be inferred from the deviation of the relaxation behavior from a single-mode Maxwellian model [55–57], and is therefore relatively unaffected by branching. The more microscopic parameters, namely, the persistence length l_p and α_e (ratio of entanglement length l_e to l_p), based on our previous findings [36–38,48], are extracted from rheological data at high frequencies at which the rheology is also insensitive to branching.

However, as illustrated by Fig. 8 (and additionally in Fig. S5 in the Supplemental Material [58]), the frequency dependence of the linear moduli G' and G'' of branched micelles is very similar to that of linear micelles. It can thus be anticipated that a given pair of G' and G'' curves can be fit equally well by either allowing for or ignoring branching, simply by adjusting other micelle parameters. Although the fit of the rheology for branched micelles using a model for linear ones gives a pseudo micelle size $\langle M\rangle$ that is much lower than the true value for the branched micelles, without knowing the extent to which topology and other micellar properties can vary with salt concentration or other solution properties, linear rheology alone is insufficient to differentiate the effect of branching from other parameters of entangled micelle solutions.

C. Estimation of degree of micellar branching

Since the linear rheology can be fit well by ignoring branches, a possible method to infer their presence is to examine the changes in linear rheology with added salt, using an assumed dependence of other micelle properties on salt concentration. Here, linear rheology of micelle solutions (with the same volume fraction $\phi = 4.02\%$) was obtained by the combination of optical microrheology and mechanical rheometry at a series of salt concentrations. A linear micelle regime of the above surfactant solutions was studied in our previous work with a similar experimental protocol [38,48,61]. Details regarding the micellar material and the associated rheological measurements can be found in the previous section.

According to Fig. 6 (inserted plot) or Fig. 9(a), a maximum in η_0, i.e., the so-called salt peak, at $[{\rm Na}^+] = 0.851$ M, was observed beyond which the effect of branching becomes dominant as confirmed by SANS [47]. We seek to quantify the topology of micelles by first fitting linear rheology data by assuming pseudo linear micelles with average length $\langle L\rangle$ as shown by the × symbols in Fig. 9(b). The corresponding estimates of other branching-independent micellar properties, i.e., reaction time $\bar{\tau}_{\rm br}$, entanglement length l_e ($= \alpha_e l_p$), and persistence length l_p, are given in Figs. 9(c) and 9(d): A decrease in l_e is observed with nearly constant l_p at high ratios of $[{\rm Na}^+]/[{\rm SLE1S} + {\rm CAPB}]$. This results in a slight increase of entanglement modulus with increasing salt concentration, indicating micelles are more densely entangled with smaller entanglement spacing, possibly due to stronger electrostatic screening at higher salt concentration.

Taking as examples two micelle systems on the right side of the salt peak, with [Na+] = 0.901 and 0.950 M (and results for other salt concentrations given in Fig. S7 in the Supplemental Material [58]), the model predictions under the assumption of linear micelles (given by the dashed lines) match well with the experimental measurements (denoted by hollow symbols) over six decades of frequency in Figs. 9(e) and 9(f). However, since we show below that similar fitting is obtained when allowing branching, additional information is required to estimate the true micelle size $\langle M\rangle$. This can be achieved by extrapolating the micelle size $\langle M\rangle = \langle L\rangle$ obtained for the two salt concentrations on the left side of the salt curve in Fig. 9(b) to the right side of the salt curve. The extrapolation is carried out here by assuming a linear dependence on salt concentration of scission free energy $E_{\rm sc}$ (i.e., the free energy to break a cylindrical micelle, creating two new endcaps) [48] using $\langle M\rangle \propto \exp(E_{\rm sc}/2k_BT)$.

This allows us to estimate the true average micelle size $\langle M\rangle$ beyond the salt peak [denoted by + in Fig. 9(b)] in contrast to the apparent decrease of the pseudo length $\langle L\rangle$ obtained when fitting without allowing branches [i.e., × symbols in Fig. 9(b)]. The branching density β can then be obtained by fitting to the experimental measurements in Figs. 9(e) and 9(f) with average strand length $\langle S\rangle$ determined by its dependence on $\langle M\rangle$ and β. Detailed values of scission free energies $E_{\rm sc}$, micelle sizes $\langle M\rangle$, strand lengths $\langle S\rangle$, and branching densities β at various $[{\rm Na}^+]$ are listed in Table S1 in the Supplemental Material [58].

As also illustrated in Figs. 9(e) and 9(f), the good fits obtained by allowing for branches (filled symbols) and the corresponding values of $\langle S\rangle$ and β indicate that obtaining branching parameters from linear rheology is under determined unless additional information is provided. The

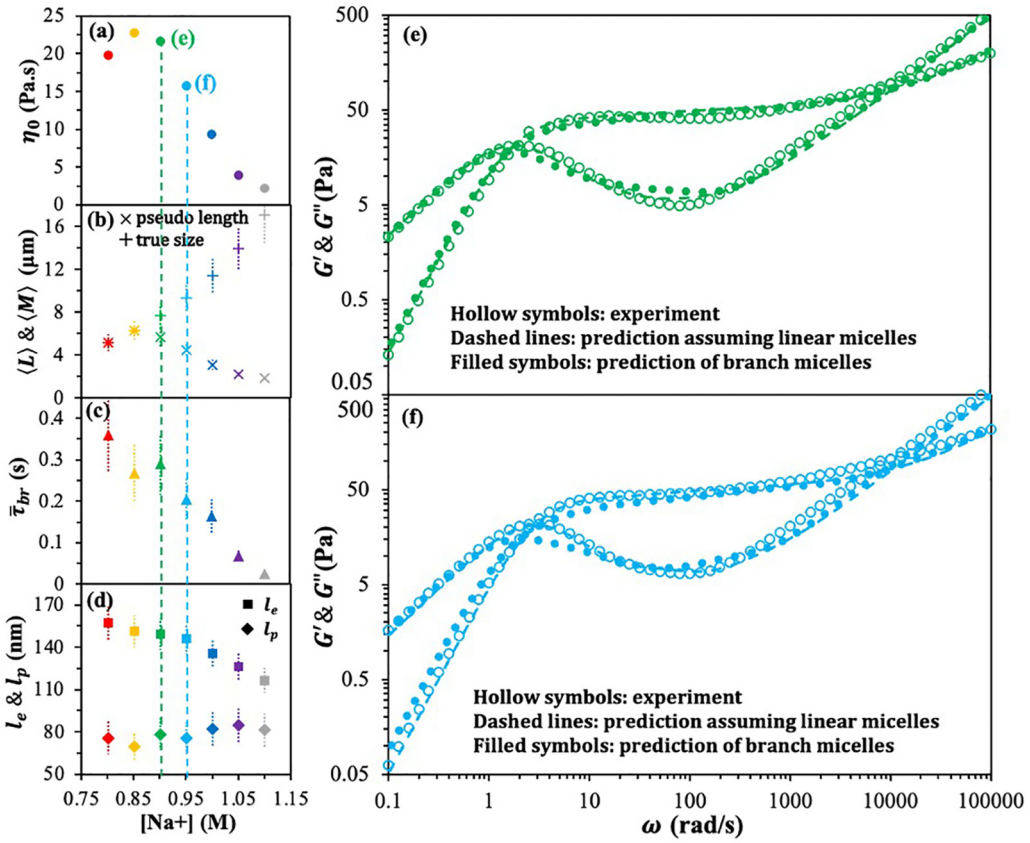

FIG. 9. (a) The experimentally measured zero-shear viscosity η_0. (b) The pseudomicelle length $\langle L \rangle$ and true micelle size $\langle M \rangle$ (from an assumed linear dependence of scission free energy E_{sc} on $[Na^+]$), (c) micellar breakage/fusion time $\bar{\tau}_{br}$, and (d) the entanglement l_e and persistence length l_p, extracted by fitting the pointer algorithm to the rheology assuming linear micelles. (e) and (f) Experimental measurements and corresponding fits assuming no branches (dashed lines) and allowing for branches (filled symbols) for rheological moduli G' and G'' of micelle solutions at 25 °C with the same surfactant volume fraction (4.04%) with (e) $[Na^+] = 0.901$ M and (f) $[Na^+] = 0.951$ M, each coded by a color also used in (a)–(d). Note that the inserted tables show the estimates for the branching-associated topological parameters: average strand length $\langle S \rangle$ and branching density β whose values are determined under the assumption that $\bar{\tau}_{br}$, l_e, and l_p are unaffected by the presence of branching. Error bars of the parameters (c) and (d) estimated from rheology are based on their insensitivity percentages. This is the percentage by which the parameter can be allowed to vary from the best-fit value while retaining an average absolute fitting error $< 10\%$, with other parameters allowed to adjust to compensate to the extent possible. (The slightly better fit to the data obtained from the linear micelle model is due to the better optimization for this model than for the more expensive branched micelle model.)

assumptions made above (i.e., that micelle scission free energy increases linearly with increasing salt concentration) provide an example of how this can be done. Of course, the method needs to be checked and possibly corrected, in case the scission free energy is not linear in salt concentration or other micelle parameters vary with salt differently than assumed here. We believe that nonlinear rheological data fitted using a nonlinear model, such as the recent adaptation of the slip-spring model to micelles proposed by Sato *et al.* [62], may provide a means to validate and improve our estimation of branching parameters.

V. CONCLUSIONS

We presented a mesoscopic model for the relaxation and linear rheology of branched micelle solutions, which we used to model the nonmonotonic dependence of viscosity on salt concentration observed for many surfactant solutions. We modeled the evolution of branched micelles by combining branch formation and dynamics with diffusion of micelles within entanglement tubes, with micellar scission and fusion reactions taken from our previously developed pointer algorithm for entangled linear micelles. Analogously with the Kirchhoff circuit model, our constrained diffusion model maps the micelle topology onto a bidirectional connectivity matrix that tracks reptation of micellar mass through branch junctions under the constraint of no accumulation of surfactant at the branch point. Branch formation from a linear segment is introduced and controlled by an associated branch budding time scale and thus offers an avenue towards analyzing micellar solutions containing very large and complex branched clusters with up to hundreds of branch points and tens of microns in size.

The result is a mesoscale simulation model for the rheology of a branched micellar solution with independent parameters to account for micelle size and topology (i.e., average strand length $\langle S \rangle$ and branching density β), reaction kinetics k_{br}, dimensionless entanglement spacing α_e, as well as the micelle

flexibility (persistence length l_p). This model allows the determination of scaling exponents for micelle solution viscosity against micelle strand length, or branching density, results that are difficult or impossible to determine experimentally. Our results clearly demonstrate shear viscosity scales differently with end and branch-point densities during the transition from linear to branched structure. The scaling exponent for viscosity as a function of strand length $\langle S \rangle$ (a strand is a portion of the micelle terminated on each end by either a micelle end or a branch point), increases dramatically for micelles with higher branching densities and thus contradicts the hypothesis that the viscosity of a solution of branched micelles is the same as that of linear micelles whose mean length equals the strand length of the branched micelles.

The model also offers a practical method for inferring properties such as micelle size, branching density, and breakage rate from their linear rheology. Assuming a linear dependence of the scission energy on the added salt concentration and that other micelle parameters including breakage time are the same as those obtained by fitting rheology using a code for linear micelles, the commonly observed decrease in solution viscosity at increased salt concentration can be fitted by allowing for increasing branching with increasing salt concentration. This demonstrates that, by fitting the experimental linear viscoelastic data (i.e., G' and G'') over a range of salt concentrations on the low-salt side of the diagram where branching can be neglected, the dependence of micelle scission free energy can be inferred and extrapolated to the high-salt side, thereby allowing the branching density as a function of salt concentration on the high-salt side to be inferred. Checking the assumptions underlying this approach, for example, using nonlinear rheological data, should be a high priority for future work. This model thus provides an important step toward establishing the structure-property relationship for entangled micellar solutions over the entire range of salt curve.

ACKNOWLEDGMENTS

The authors acknowledge support from the National Science Foundation (NSF; under Grants No. CBET-1500377 and No. CBET-1907517) and discussions with Mike Cates of University of Cambridge and Xueming Tang of the University of Michigan (now at 3M). Any opinions, findings, and conclusions or recommendations expressed in this material are those of the authors and do not necessarily reflect the views of NSF.

[1] M. E. Cates and S. M. Fielding, Rheology of giant micelles, Adv. Phys. **55**, 799 (2006).

[2] M. E. Helgeson, T. K. Hodgdon, E. W. Kaler, N. J. Wagner, M. Vethamuthu, and K. P. Ananthapadmanabhan, Formation and rheology of viscoelastic "double networks" in wormlike micelle-nanoparticle mixtures, Langmuir **26**, 8049 (2010).

[3] M. Ouchi, T. Takahashi, and M. Shirakashi, Shear-induced structure change and flow-instability in start-up Couette flow of aqueous, wormlike micelle solution, J. Rheol. **50**, 341 (2006).

[4] T. Tlusty and S. A. Safran, Defect-induced phase separation in dipolar fluids, Science **290**, 1328 (2000).

[5] G. Z. Waton and R. Zana, Relaxation in wormlike micelle solutions, in *Giant Micelles: Properties and Applications*, 1st ed., edited by R. Zana and E. W. Kaler (CRC Press, Boca Raton, 2007).

[6] M. Youssry, E. Lemaire, B. Caillard, A. Colin, and I. Dufour, On-chip characterization of the viscoelasticity of complex fluids using microcantilevers, Meas. Sci. Technol. **23**, 125306 (2012).

[7] A. Bernheim-Groswasser, E. Wachtel, and Y. Talmon, Micellar growth, network formation, and criticality in aqueous solutions of the nonionic surfactant $C_{12}E_5$, Langmuir **16**, 4131 (2000).

[8] R. D. Koehler, S. R. Raghavan, and E. W. Kaler, Microstructure and dynamics of wormlike micellar solutions formed by mixing cationic and anionic surfactants, J. Phys. Chem. B **104**, 11035 (2000).

[9] E. K. Wheeler, P. Izu, and G. G. Fuller, Structure and rheology of wormlike micelles, Rheol. Acta **35**, 139 (1996).

[10] V. A. Andreev and A. I. Victorov, Molecular thermodynamics for micellar branching in solutions of ionic surfactants, Langmuir **22**, 8298 (2006).

[11] J. J. Cardiel, Y. Zhao, P. De La Iglesia, L. D. Pozzo, and A. Q. Shen, Turning up the heat on wormlike micelles with a hydrotopic salt in microfluidics, Soft Matter **10**, 9300 (2014).

[12] D. Gaudino, R. Pasquino, and N. Grizzuti, Adding salt to a surfactant solution: Linear rheological response of the resulting morphologies, J. Rheol. **59**, 1363 (2015).

[13] S. Jain and F. S. Bates, On the origins of morphological complexity in block copolymer surfactants, Science **300**, 460 (2003).

[14] A. Zilman, S. A. Safran, T. Sottmann, and R. Strey, Temperature dependence of the thermodynamics and kinetics of micellar solutions, Langmuir **20**, 2199 (2004).

[15] N. Dan and S. A. Safran, Junctions and end-caps in self-assembled non-ionic cylindrical micelles, Adv. Colloid Interface Sci. **123**, 323 (2006).

[16] J. T. Kindt, Simulation and theory of self-assembled networks: Ends, junctions, and loops, J. Phys. Chem. B **106**, 8223 (2002).

[17] T. Tlusty, S. A. Safran, and R. Strey, Topology, phase instabilities, and wetting of microemulsion networks, Phys. Rev. Lett. **84**, 1244 (2000).

[18] J. J. Cardiel, A. C. Dohnalkova, N. Dubash, Y. Zhao, P. Cheung, and A. Q. Shen, Microstructure and rheology of a flow-induced structured phase in wormlike micellar solutions, Proc. Natl. Acad. Sci. USA **110**, E1653 (2013).

[19] S. A. Rogers, M. A. Calabrese, and N. J. Wagner, Rheology of branched wormlike micelles, Curr. Opin. Colloid Interface Sci. **19**, 530 (2014).

[20] T. N. Stancheva, M. T. Georgiev, G. M. Radulova, K. D. Danov, and K. G. Marinova, Rheology of saturated micellar networks: Wormlike micellar solutions vs. bicontinuous micellar phases, Colloids Surf. A **652**, 129927 (2022).

[21] P. Koshy, V. K. Aswal, M. Venkatesh, and P. A. Hassan, Unusual scaling in the rheology of branched wormlike

micelles formed by cetyltrimethylammonium bromide and sodium oleate, J. Phys. Chem. B **115**, 10817 (2011).
[22] M. S. Turner and M. E. Cates, Linear viscoelasticity of wormlike micelles: A comparison of micellar reaction kinetics, J. Phys. II France **2**, 503 (1992).
[23] J. T. Padding, E. S. Boek, and W. J. Briels, Dynamics and rheology of wormlike micelles emerging from particulate computer simulations, J. Chem. Phys. **129**, 074903 (2008).
[24] C. Zhang and J. Wei, Mesoscale simulation study of the structure and rheology of dilute solutions of flexible micelles, Chem. Eng. Sci. **102**, 544 (2013).
[25] A. G. Zilman and S. A. Safran, Thermodynamics and structure of self-assembled networks, Phys. Rev. E **66**, 051107 (2002).
[26] M. In, G. G. Warr, and R. Zana, Dynamics of branched threadlike micelles, Phys. Rev. Lett. **83**, 2278 (1999).
[27] J. Appell, G. Porte, A. Khatory, F. Kern, and S. J. Candau, Static and dynamic properties of a network of wormlike surfactant micelles (cetylpyridinium chlorate in sodium chlorate brine), J. Phys. II France **2**, 1045 (1992).
[28] J. K. Riley, J. J. Richards, N. J. Wagner, and P. D. Butler, Branching and alignment in reverse worm-like micelles studied with simultaneous dielectric spectroscopy and RheoSANS, Soft Matter **14**, 5344 (2018).
[29] G. Porte, J. Appell, and Y. Poggi, Experimental investigations on the flexibility of elongated cetylpyridinium bromide micelles, J. Phys. Chem. **84**, 3105 (1980).
[30] D. Sachsenheimer, C. Oelschlaeger, S. Müller, J. Küstner, S. Bindgen, and N. Willenbacher, Elongational deformation of wormlike micellar solutions, J. Rheol. **58**, 2017 (2014).
[31] J. F. Berret, J. Appell, and G. Porte, Linear rheology of entangled wormlike micelles, Langmuir **9**, 2851 (1993).
[32] T. J. Drye and M. E. Cates, Living networks: The role of crosslinks in entangled surfactant solutions, J. Chem. Phys. **96**, 1367 (1992).
[33] R. G. Larson, The lengths of thread-like micelles inferred from rheology, J. Rheol. **56**, 1363 (2012).
[34] D. Angelescu, A. Khan, and H. Caldararu, Viscoelastic properties of sodium dodecyl sulfate with aluminum salt in aqueous solution, Langmuir **19**, 9155 (2003).
[35] S. R. Raghavan, G. Fritz, and E. W. Kaler, Wormlike micelles formed by synergistic self-assembly in mixtures of anionic and cationic surfactants, Langmuir **18**, 3797 (2002).
[36] W. Zou and R. G. Larson, A mesoscopic simulation method for predicting the rheology of semi-dilute wormlike micellar solutions, J. Rheol. **58**, 681 (2014).
[37] W. Zou, X. Tang, M. Weaver, P. Koenig, and R. G. Larson, Determination of characteristic lengths and times for wormlike micelle solutions from rheology using a mesoscopic simulation method, J. Rheol. **59**, 903 (2015).
[38] X. Tang, W. Zou, P. H. Koenig, S. D. McConaughy, M. R. Weaver, D. M. Eike, M. J. Schmidt, and R. G. Larson, Multiscale modeling of the effects of salt and perfume raw materials on the rheological properties of commercial threadlike micellar solutions, J. Phys. Chem. B **121**, 2468 (2017).
[39] S. May, Y. Bohbot, and A. Ben-Shaul, Molecular theory of bending elasticity and branching of cylindrical micelles, J. Phys. Chem. B **101**, 8648 (1997).
[40] M. A. Calabrese and N. J. Wagner, Detecting branching in wormlike micelles via dynamic scattering methods, ACS Macro Letters **7**, 614 (2018).
[41] M. Chellamuthu and J. P. Rothstein, Distinguishing between linear and branched wormlike micelle solutions using extensional rheology measurements, J. Rheol. **52**, 865 (2008).
[42] D. Danino, Y. Talmon, H. Levy, G. Beinert, and R. Zana, Branched threadlike micelles in an aqueous solution of a trimeric surfactant, Science **269**, 1420 (1995).
[43] J. P. Decruppe and A. Ponton, Flow birefringence, stress optical rule and rheology of four micellar solutions with the same low shear viscosity, Eur. Phys. J. E **10**, 201 (2003).
[44] M. E. Helgeson, P. A. Vasquez, E. W. Kaler, and N. J. Wagner, Rheology and spatially resolved structure of cetyltrimethylammonium bromide wormlike micelles through the shear banding transition, J. Rheol. **53**, 727 (2009).
[45] S. W. Holder, S. C. Grant, and H. Mohammadigoushki, Nuclear magnetic resonance diffusometry of linear and branched wormlike micelles, Langmuir **37**, 3585 (2021).
[46] S. Wu and H. Mohammadigoushki, Linear versus branched: Flow of a wormlike micellar fluid past a falling sphere, Soft Matter **17**, 4395 (2021).
[47] K. Vogtt, G. Beaucage, K. Rishi, H. Jiang, and A. Mulderig, Hierarchical approach to aggregate equilibria, Phys. Rev. Res. **1**, 033081 (2019).
[48] W. Zou, G. Tan, H. Jiang, K. Vogtt, M. Weaver, P. Koenig, G. Beaucage, and R. G. Larson, From well-entangled to partially-entangled wormlike micelles, Soft Matter **15**, 642 (2019).
[49] D. Danino, Y. Talmon, and R. Zana, Cryo-TEM of thread-like micelles: On-the-grid microstructural transformations induced during specimen preparation, Colloids Surf. A **169**, 67 (2000).
[50] S. Yamamoto and S.-a. Hyodo, Mesoscopic simulation of the crossing dynamics at an entanglement point of surfactant threadlike micelles, J. Chem. Phys. **122**, 204907 (2005).
[51] P. Fischer, G. G. Fuller, and Z. Lin, Branched viscoelastic surfactant solutions and their response to elongational flow, Rheol. Acta **36**, 632 (1997).
[52] A. Khatory, F. Kern, F. Lequeux, J. Appell, G. Porte, N. Morie, A. Ott, and W. Urbach, Entangled versus multiconnected network of wormlike micelles, Langmuir **9**, 933 (1993).
[53] F. Lequeux, Reptation of connected wormlike micelles, EPL **19**, 675 (1992).
[54] M. Tang and W. C. Carter, Branching mechanisms in surfactant micellar growth, J. Phys. Chem. B **117**, 2898 (2013).
[55] M. E. Cates, Dynamics of living polymers and flexible surfactant micelles: Scaling laws for dilution, J. Phys. France **49**, 1593 (1988).
[56] M. E. Cates and S. J. Candau, Statics and dynamics of wormlike surfactant micelles, J. Phys. Condens. Matter **2**, 6869 (1990).
[57] R. Granek, Dip in $G''(\omega)$ of polymer melts and semidilute solutions, Langmuir **10**, 1627 (1994).
[58] See Supplemental Material at http://link.aps.org/supplemental/10.1103/PhysRevResearch.5.043024 for data processing, simulation setup, as well as other details regarding the scaling behaviors and quantification of branching.
[59] C. Oelschlaeger, M. Schopferer, F. Scheffold, and N. Willenbacher, Linear-to-branched micelles transition: A rheometry and diffusing wave spectroscopy (DWS) study, Langmuir **25**, 716 (2009).
[60] F. Lequeux and S. J. Candau, Dynamical properties of wormlike micelles: Deviations from the "classical" picture, in *Structure and Flow in Surfactant Solutions*, ACS Symposium Series

(American Chemical Society, Washington, DC, 1994), Vol. 578, pp. 51–62.

[61] G. Tan, W. Zou, M. Weaver, and R. G. Larson, Determining threadlike micelle lengths from rheometry, J. Rheol. **65**, 59 (2021).

[62] T. Sato, S. Moghadam, G. Tan, and R. G. Larson, A slip-spring simulation model for predicting linear and nonlinear rheology of entangled wormlike micellar solutions, J. Rheol. **64**, 1045 (2020).